Nuclear Instruments and Methods in Physics Research A272 (1988) 695–706
North-Holland, Amsterdam

PERFORMANCE OF A SCINTILLATING GLASS CALORIMETER FOR ELECTROMAGNETIC SHOWERS

U. BUCHNER, J.P. DONKER, B. SPAAN, J. SPENGLER *, G. SCHWEDA and D. WEGENER
Institut für Physik, Universität Dortmund, Dortmund, FRG

W. SCHMIDT-PARZEFALL
DESY, Hamburg, FRG

Received 6 May 1988

Dedicated to Ulrich Bonse on the occasion of his 60th birthday

A scintillating glass electromagnetic calorimeter consisting of 3×3 moduls of $8\times8\times66$ cm^3 each has been studied with electrons in the energy interval 14.7 MeV $< E <$ 6000 MeV. An energy resolution of $\sigma_E/E[\%] = \sqrt{1.6^2/E[\mathrm{GeV}] + 1.0^2}$ was achieved. The spatial resolution turns out to be of the order $\sigma = 4$ to 8 mm depending on the impact point and the angle of incidence; it improves with increasing energy. The observations are in excellent agreement with the result of an EGS Monte Carlo simulation of the detector including optical effects and photoelectron statistics.

1. Introduction

The new generation of detectors proposed for B-factories include a powerful electromagnetic calorimeter which combines good energy and spatial resolution with large efficiency for low energy (> 10 MeV) photon detection [1,2]. In addition the detector material should have a high radiation resistance and the mechanical handling should be easy. Scintillating glasses are potentially capable of yielding in the energy region of interest a resolution comparable to CsI(Tl) [3,4] and BGO [5] at a much lower price. We have built and tested an array of 3×3 scintillating glass blocks with an area of 8×8 cm^2 and a length of 66 cm each. The response of this electromagnetic calorimeter to electrons with energies of 14.7 MeV $< E <$ 6000 MeV has been studied. We report on the optical properties, the long term behaviour and on the energy and spatial resolution achieved. The measurements are compared to Monte Carlo simulations of the detector.

2. Optical properties of the scintillating glass

The composition of the scintillating glass HED-1 used in this experiment is shown in table 1 [6]. The small component of K_2O produces an activity of 2.6 Bq/cm^3, which is negligible for our purposes. The radiation length is mainly determined by BaO while the scintillating component is Ce_2O_3. The parameters characterizing the electromagnetic shower development in the glass are collected in table 2. For comparison the corresponding values of the scintillating glass SCG1-C [7], whose properties have been extensively studied in other experiments [8–13] are included.

Three factors determine the energy resolution of a homogeneous calorimeter namely intrinsic shower fluctuations, leakage fluctations and the amount of light produced in the shower counter [14]. The number of photons n_γ per MeV energy deposited is therefore of great interest. However, this number is not directly

Table 1
Composition of HED-1

	Contents [wt.%]
BaO	44.2
SiO_2	42.0
MgO	4.0
Li_2O	3.8
K_2O	3.0
Ce_2O_3	1.6
P_2O_5	1.2
LiF	0.5

* Now at DESY, Hamburg, FRG.

Table 2
Properties of different counter materials; the numbers given for HED-1 have been determined in the present experiment

	HED-1	SCG1-C	SF5	SF6	CsI(Tl)
ρ [g/cm^3]	3.44	3.49 [9]	4.07 [6]	5.18 [6]	4.53 [3]
X_0 [cm]	4.12	4.12 [9]	2.55 [6]	1.70 [6]	1.85 [3]
R_M [cm]	3.9		3.17	2.70	3.8 [5]
ϵ_c [MeV]	22.0		16.9 [6]	13.1 [6]	10.2 [5]
n_d (587.6 nm)	1.609		1.673 [6]	1.805 [6]	
decay const. [ns]	87 ± 5	70 [9]			1000 [3]
λ_{peak} [nm]	435	430 [9]			
n_{pe}/MeV	12.5 ± 1.2	3 ± 0.2 [13]	0.6 ± 0.05	0.9 ± 0.1	
n_γ/MeV	330 ± 42	100 ± 20 [13]			4.5×10^4 [5]

accessible to experiments, in contrast to the number of photoelectrons n_{pe} produced at the cathode of the photomultiplier, which represents the effective light output of the counter. To derive n_γ, the emission spectrum, the optical absorption length μ_{op} and the refractive index of the material have to be known.

The fluorescence spectrum (fig. 1) of a $3 \times 3 \times 3$ cm^3 glass block excited with UV light was measured using a monochromator [15]. The absorption of this glass block was studied in a transmission experiment. The resulting transmission curve is included in fig. 1. The spectral distributions fit nicely with the spectral efficiency of standard phototubes.

The technical absorption length μ_t of the glass was determined with the setup shown in fig. 2 [16]. An electron beam ($E = 3$ GeV) entered a shower counter module in its lateral plane at a given distance z from the photomultiplier tube (Valvo XP 3462B). In fig. 2 the measured peak values of the pulse height spectra are plotted as a function of the distance z between the impact point and the cathode plane of the phototube. Two components are expected to contribute: the light emitted in the direction of the phototube plus the component emitted into the opposite direction and reflected at the end of the module opposite to the phototube. Hence one expects the following dependence of the light output as a function of z:

$$I = I_0\left[(1-d)\exp\left(-\frac{2c-z}{\mu_t}\right) + d\exp\left(\frac{-z}{\mu_t}\right)\right], \qquad (1)$$

where c denotes the length of the glass block. Deviations of the data from eq. (1) are expected at small distances $z < 10$ cm, due to the large contribution of direct light. Fitting expression (1) to the measured data (fig. 2) ($z > 10$ cm) one gets

$$\mu_t = 77 \pm 8 \text{ cm}. \qquad (2)$$

The observed distribution can be reproduced by a Monte Carlo calculation taking into account the total reflection, the reflection at the aluminium foils covering the scintillating glass modules and the absorption length of the light in the glass of $\langle \mu_{op} \rangle = 89$ cm. The latter

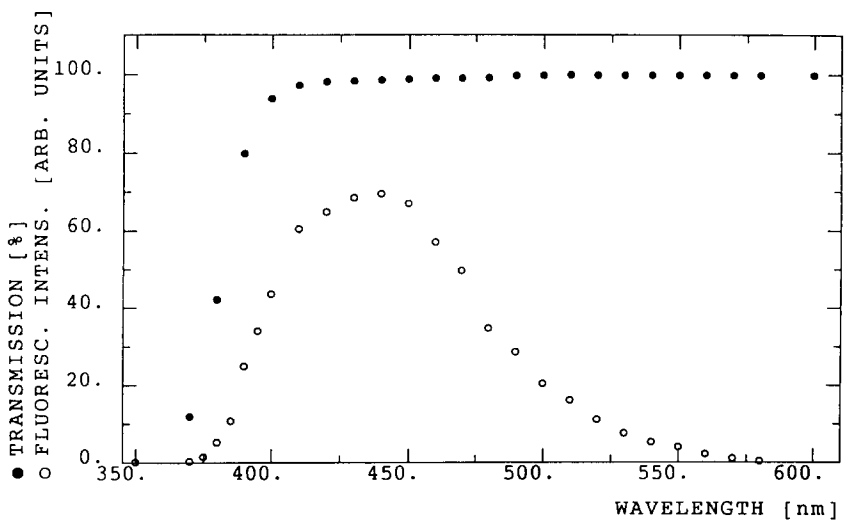

Fig. 1. Fluorescence spectrum (open circles) and transmission spectrum (black dots) of a HED-1 glass block of $3 \times 3 \times 3$ cm^3.

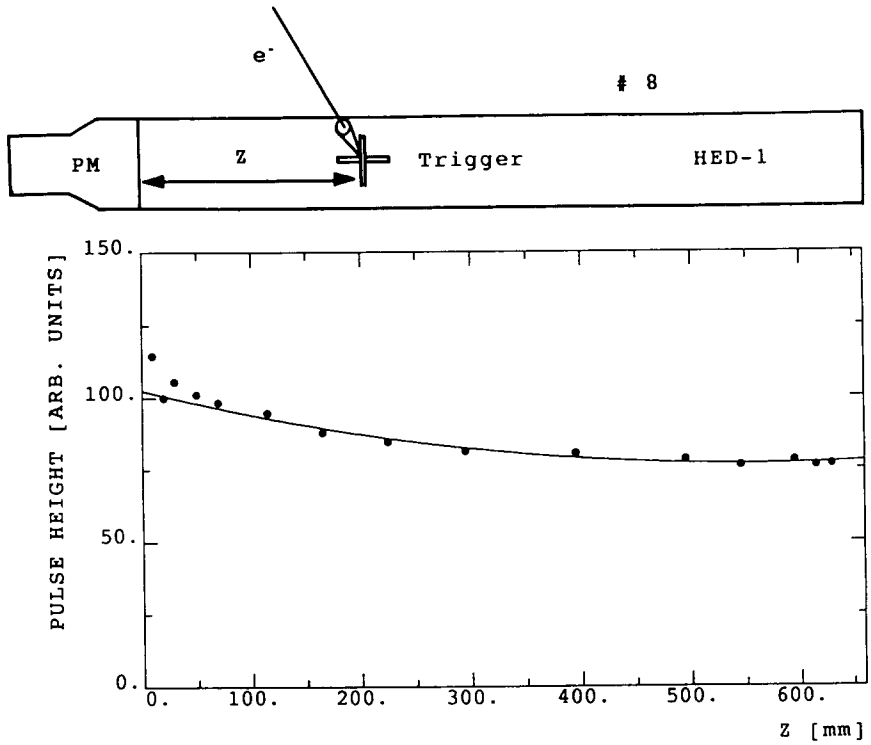

Fig. 2. Light collection as a function of the distance from the photomultiplier.

value is compatible with the optically determined absorption length [16]. This result demonstrates that the simulation of the light collection used in the present analysis is well under control.

We have exploited the possibility to simulate the light production and collection to determine the effective number of photons per MeV deposited energy produced by a minimum ionizing particle in the glass:

$$n_\gamma = \frac{n_{pe}}{\epsilon_{pe}\epsilon_{col}}, \tag{3}$$

where

n_γ = effective number of photons produced,
n_{pe} = number of photoelectrons detected,
ϵ_{pe} = photocathode efficiency,
ϵ_{col} = light collection efficiency.

Due to the longitudinal shower development, ϵ_{col} will slightly increase with the energy of the incoming particles.

Three independent measurements lead to consistent results. The number of photoelectrons produced by cosmic rays in a glass block of $3 \times 3 \times 3$ cm^3 amounts to 29 ± 3 photoelectrons per MeV deposited energy. Considering the photocathode efficiency and simulating the light collection in the glass block we arrive at a number of 270 ± 46 photons produced per MeV in the glass block. A similar measurement of the number of photoelectrons per MeV deposited by a high energy electromagnetic shower ($E = 3$ GeV) (see section 3.2 for details) yields 12.5 photoelectrons/MeV. Simulating the shower process and the light collection for this geometry one derives a number of 325 ± 65 photons per MeV. The average photocathode efficiency has been determined to $\epsilon_{pe} = 0.22 \pm 0.02$. The light collection efficiency is $\epsilon_{col} = 0.12 \pm 0.005$ at 40 MeV and 0.174 ± 0.014 at 3 GeV electron energy for a glass block of $8 \times 8 \times 66$ cm^3. A third method employed to determine this number follows from the study of the energy resolution of the electromagnetic calorimeter at low energies (15–42 MeV) as discussed in detail in section 3.4. From this analysis a number of $n_\gamma = 335 \pm 51$/MeV is derived. Comparing this light output with other presently used shower detectors (table 2) demonstrates the improvement to be expected from the use of the new material.

3. Calorimetry

3.1. Experimental setup

The measurements have been performed with a 3×3 matrix of scintillating glass counters of $8 \times 8 \times 66$ cm^3 each. The modules were wrapped separately into an

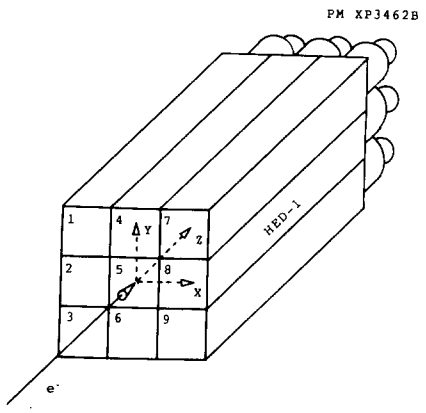

Fig. 3. Layout of the calorimeter setup in the test beam.

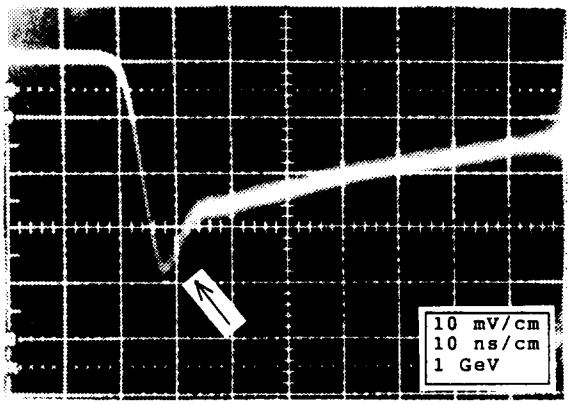

Fig. 4. Scintillation pulse recorded with an oscilloscope.

aluminium foil and covered by a light tight shrinking tube. Each module was viewed from one end by a phototube (Valvo XP 3462B), the gain of the tube was monitored by a LED fixed in front of the photomultiplier. An artists view of the setup is shown in fig. 3. Measurements were performed with electrons at the DESY synchrotron (1 GeV $< E <$ 6 GeV) [15] and at the betatron of Dortmund University (15 MeV $< E <$ 43 MeV) [16], which allowed to study the response of the shower counter in the whole energy interval of interest for a B-factory. The impact point of the beam was defined by two crossed scintillation counters to an area of 0.5×0.5 cm^2. The data were recorded by CAMAC ADCs [17]. They have been corrected for the small nonlinearity of the ADC response, which was determined separately with a pulser. The modules were intercalibrated by determining separately their response for central impact of the electron beam.

3.2. Energy response

Two components of light are expected to contribute to the observed signal: a fast pulse due to Cherenkov radiation and slower component due to scintillation light. Both components are observed as shown by the signal detected with an oscilloscope (fig. 4). The narrow spike is due to Cherenkov radiation followed by an exponential decay of the scintillation light with a lifetime of 87 ± 5 ns. The graphical integration of this signal shows that $< 10\%$ of the total signal is due to Cherenkov radiation. Note that this interpretation of the spike was checked by analyzing the data collected with the setup of fig. 2, where indeed no spike was observed.

A typical pulse height spectrum recorded at an energy of 3 GeV is shown in fig. 5. For comparison, the results of an EGS Monte Carlo calculation [18] are

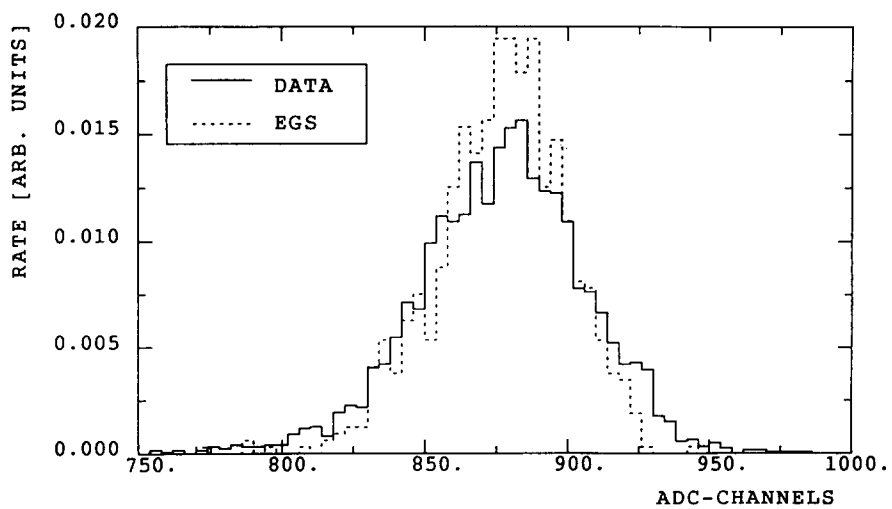

Fig. 5. Pulse height spectrum of the central counter at an energy of 3 GeV (full histogram) and the EGS simulation (dashed histogram).

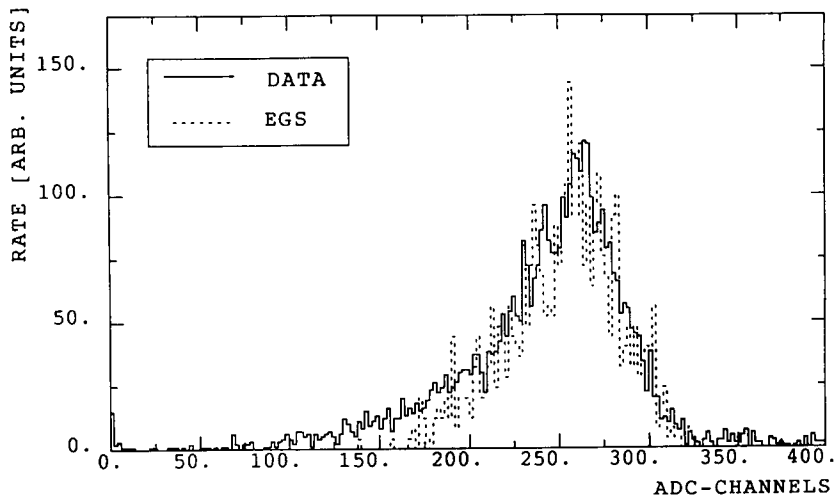

Fig. 6. Pulse height spectrum of the central counter at an energy of 42.5 MeV (full histogram) and the EGS simulation (dashed histogram).

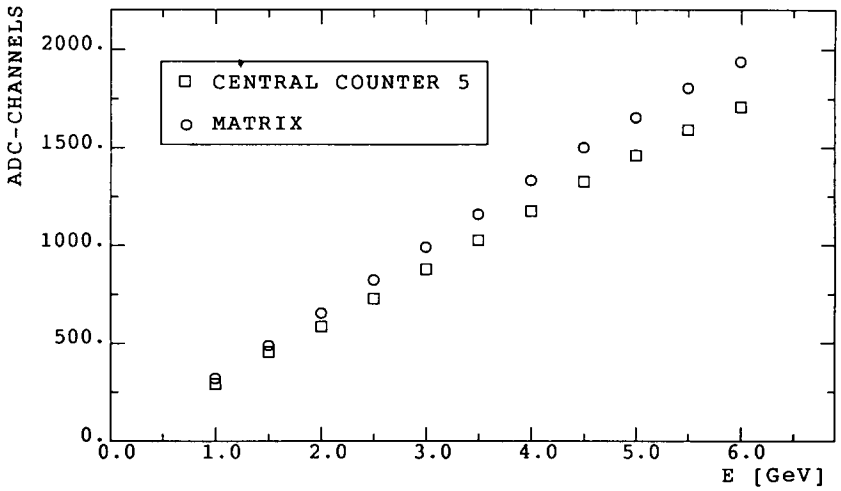

Fig. 7. Measured mean pulse height as a function of the electron energy for the central counter (open squares) and the whole matrix (circles).

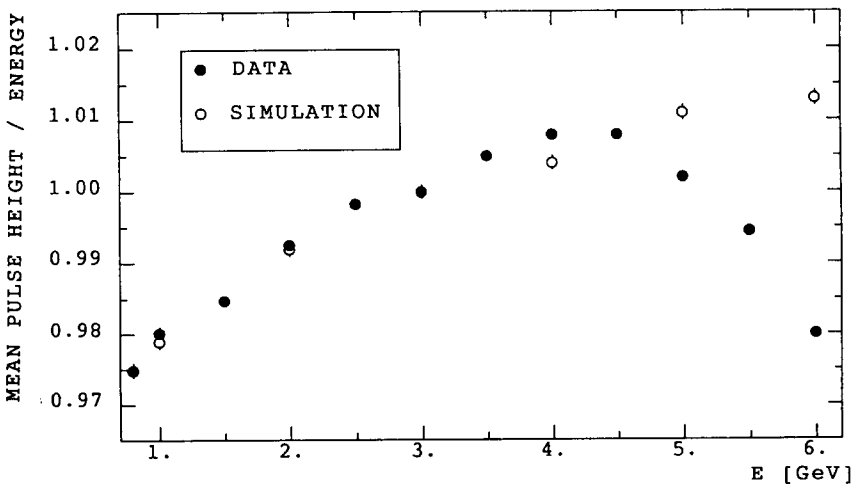

Fig. 8. Measured mean pulse height normalized to 3 GeV as a function of the electron energy for data (black circles) and the EGS simulation (open circles).

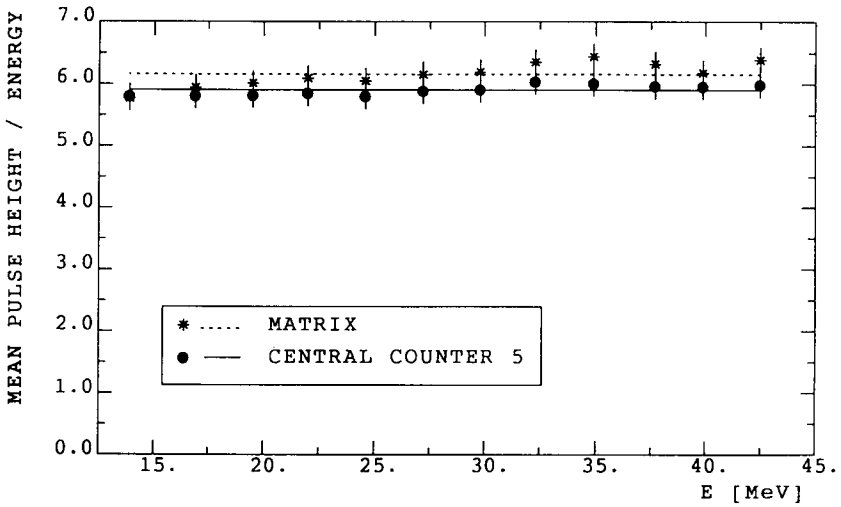

Fig. 9. Measured mean pulse height per MeV as a function of the electron energy for the central counter (black circles) and the whole matrix (stars).

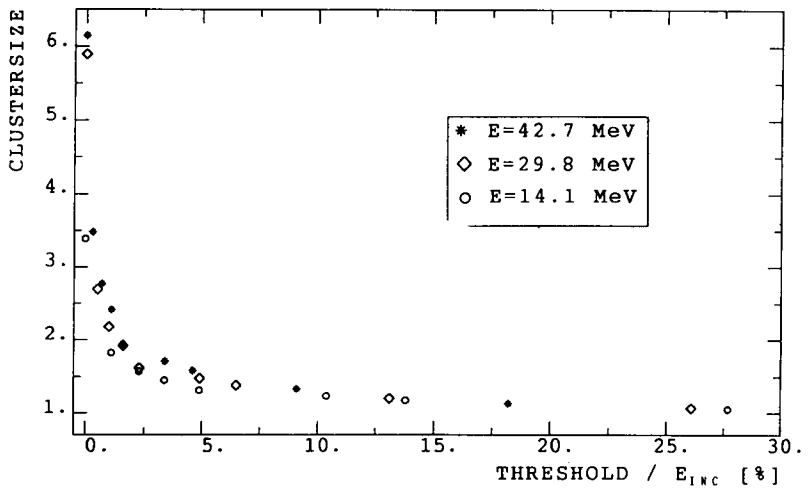

Fig. 10. Number of shower counter modules exceeding the threshold as a function of the threshold normalized to the energy of the incoming particles.

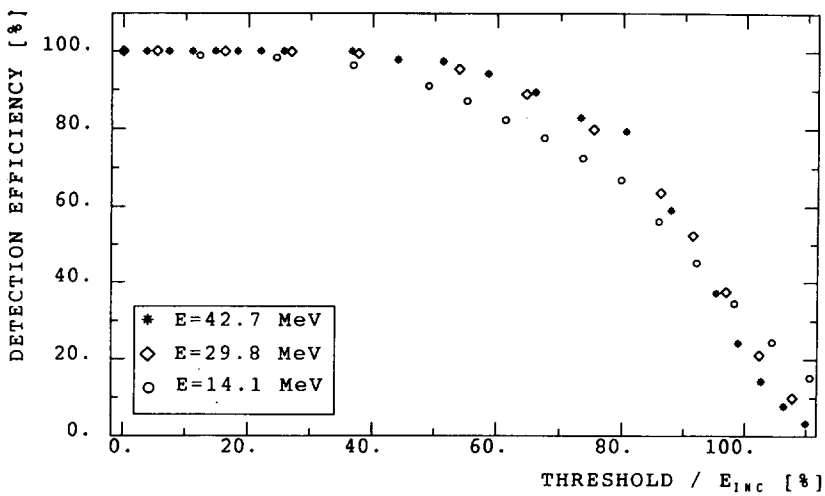

Fig. 11. Detection efficiency as a function of the threshold normalized to the energy of the incoming particles.

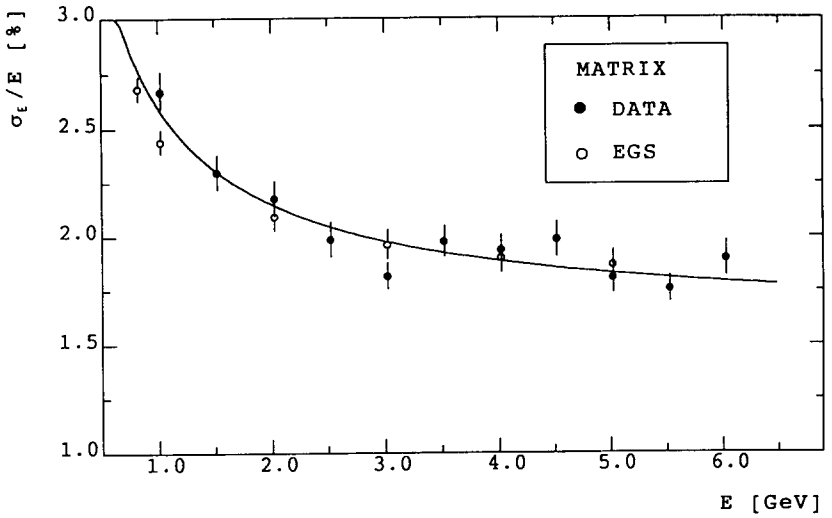

Fig. 12. Energy resolution as a function of the electron energy (black circles) and the EGS prediction (open circles). The line shows the parametrization (4) described in the text.

included, which do not include contributions of the limited beam resolution. In fig. 6 the corresponding distribution at low energy is given. In this case it is necessary to consider in the simulation not only the shower – but also the light-collection process in some detail. The discrepancy at low pulse heights can be traced back to multiple scattering in the trigger counters.

The measured pulse height energy relation is shown in fig. 7 for the central counter and for the whole matrix. After normalizing to 3 GeV, a nonlinearity of 1–2% is observed (fig. 8). It is well reproduced by the EGS simulation including optical effects in the energy interval of 1 to 4 GeV and can be attributed to the light collection (fig. 2). The discrepancy above 4 GeV between the simulation and the measurements is due to saturation effects in the dipole magnets of the testbeam. For the low energy data the ratio of the pulse height and the energy is plotted as a function of the energy (fig. 9); this ratio is indeed constant for a single counter but a deviation is observed for the matrix for energies below 30 MeV. This trend is reproduced by the full Monte Carlo calculation including the shower simulation (EGS), the light collection and the statistics of photoelectron production. The observed deviation from linearity at very low energies can be explained by the

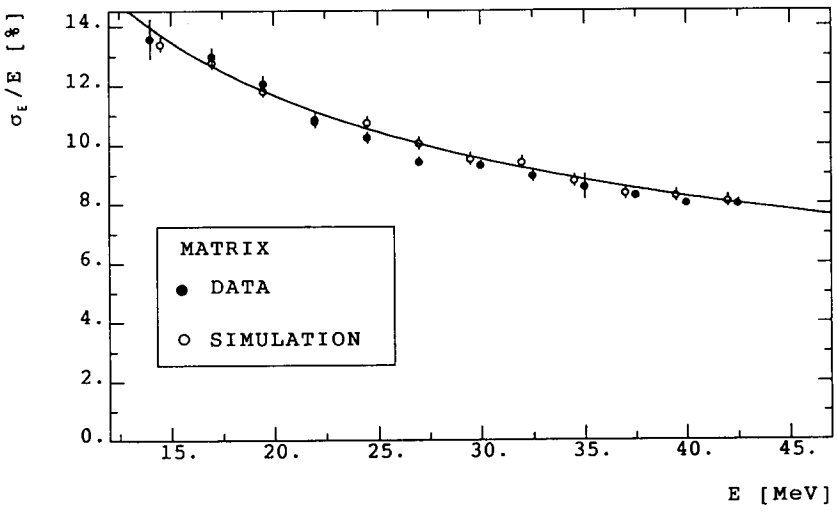

Fig. 13. Energy resolution as a function of the electron energy (black circles) and the EGS prediction (open circles) including light collection. The line shows the parametrization (5) described in the text.

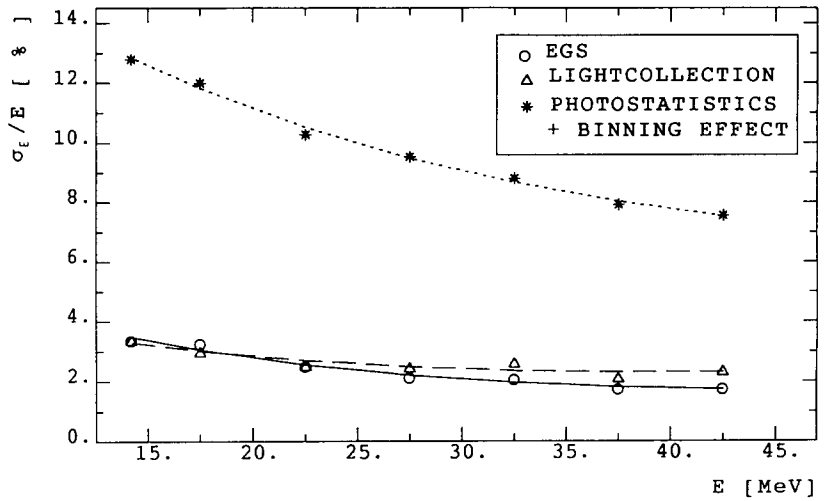

Fig. 14. Different contributions to the energy resolution as a function of the electron energy.

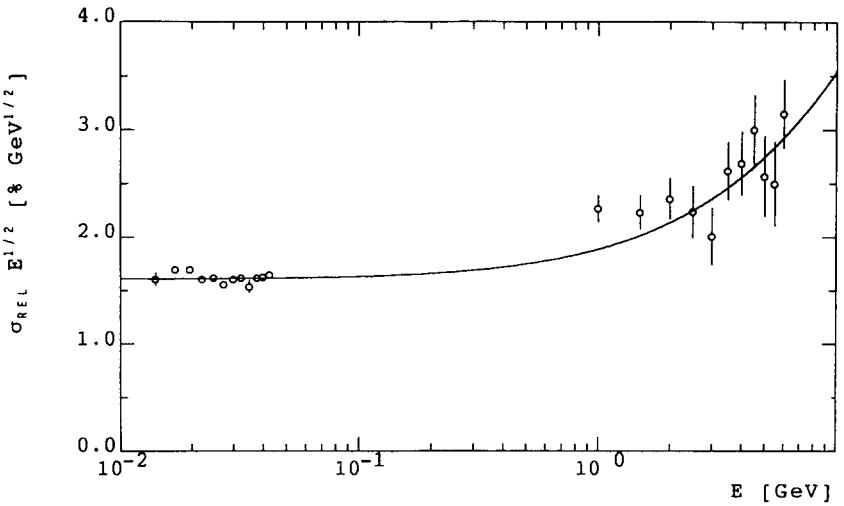

Fig. 15. Measured normalized energy resolution as a function of the electron energy. The line corresponds to the parametrization (6).

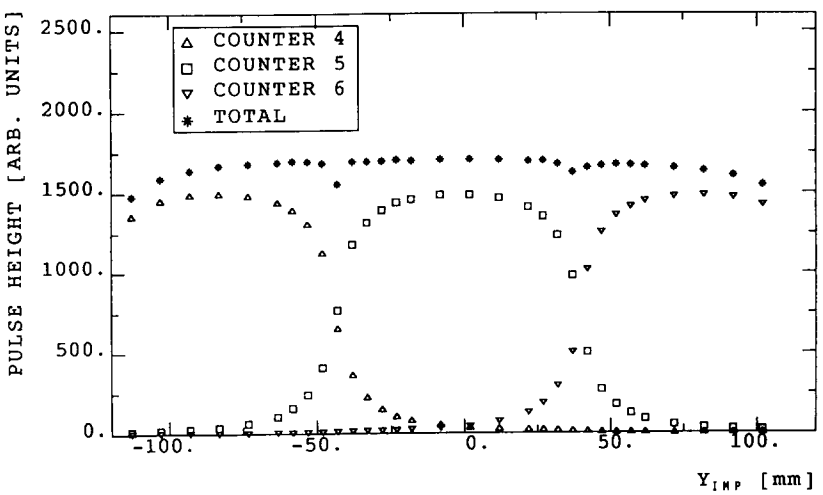

Fig. 16. Measured average pulse height as a function of the impact point for 3 GeV.

binomial statistics of photoelectron production and the digitization of the ADC. Since the energy is mainly deposited in the central counter hit by the beam particle, this binning effect is of special importance for the neighbouring counters. Therefore the nonlinearity is only observed for the summed signal of the whole detector matrix.

3.3. Performance and efficiency

In a large detector, where thousands of shower counter modules are used, a readout threshold is necessary to avoid contributions from electronical noise or from instabilities of the ADC pedestal. Only those shower counters are read out, whose pulse height is above a threshold after subtraction of the pedestal value. The performance of a calorimeter is disturbed by this threshold cut because of the following reasons:

- The number of counters showing a pulse height above threshold (cluster size) is reduced with increasing threshold (fig. 10). This has a strong influence on the spatial resolution of the calorimeter (see section 3.5).
- The reduction in cluster size corresponds to a reduction of the measured energy. This effect, which is nonnegligible for energies below 200 MeV, has to be corrected by the analysis software.
- The loss of energy leads in an additional contribution to the energy resolution.
- The detection efficiency can be influenced for very low energies as demonstrated in fig. 11. A particle is "detected", when the energy deposition in at least one shower counter exceeds the threshold.

3.4. Energy resolution

The energy resolution measured at high energies ($E > 1$ GeV) is shown in fig. 12. The data are compared to the expected resolution as derived from the EGS Monte Carlo simulation of the shower process taking into account the uncertainty of the beam resolution of $\sigma_{\text{beam}} = (1.4 \pm 0.1)\%$. The full line shown in fig. 12 corresponds to a parametrization of the form

$$\frac{\sigma_E}{E}[\%] = \sqrt{(1.0 \pm 0.12)^2 + \sigma_{\text{beam}}^2 + \frac{(2.1 \pm 0.15)^2}{E[\text{GeV}]}}\,. \tag{4}$$

The measured energy resolution at low energies is compared to the expected value of the full Monte Carlo simulation in fig. 13, which includes EGS shower development, light collection and fluctuations in the photoelectron production. Note that the uncertainty due to the energy resolution of the beam is less than 1% and can be neglected. The full line included into fig. 13 corresponds to the parametrization

$$\frac{\sigma_E}{E}[\%] = \frac{1.6 \pm 0.08}{\sqrt{E[\text{GeV}]}}\,. \tag{5}$$

The calculated resolution depends sensitively on the number of effective photons produced per MeV, hence one can derive from this measurement the corresponding number. As discussed in section 2 the result agrees perfectly with the number derived from other more direct methods. In fig. 14 the different contributions influencing the energy resolution are shown separately. It follows that at low energies the achievable resolution is dominated by photoelectron statistics and the binning effect. Adding up these terms in quadrature, the Monte Carlo prediction shown in fig. 13 is obtained. In fig. 15 the normalized energy resolution has been plotted for the whole energy range. The beam resolution of $\sigma_{\text{beam}} =$

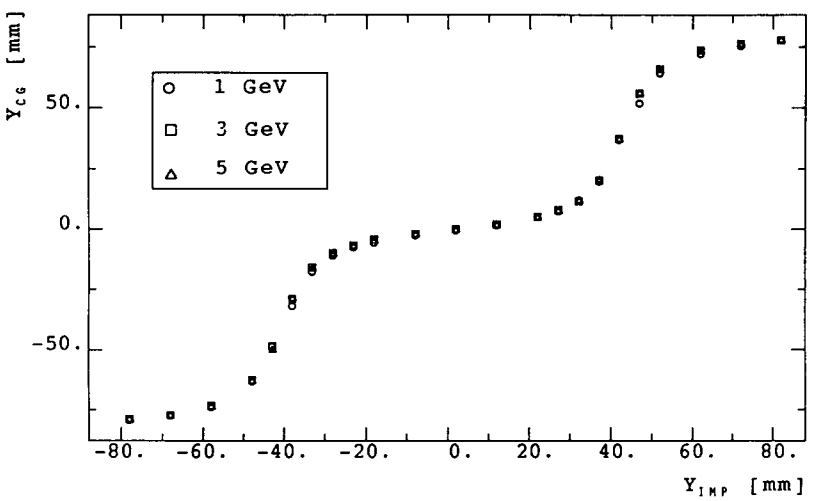

Fig. 17. Reconstructed centre of gravity as a function of the impact point for three different energies.

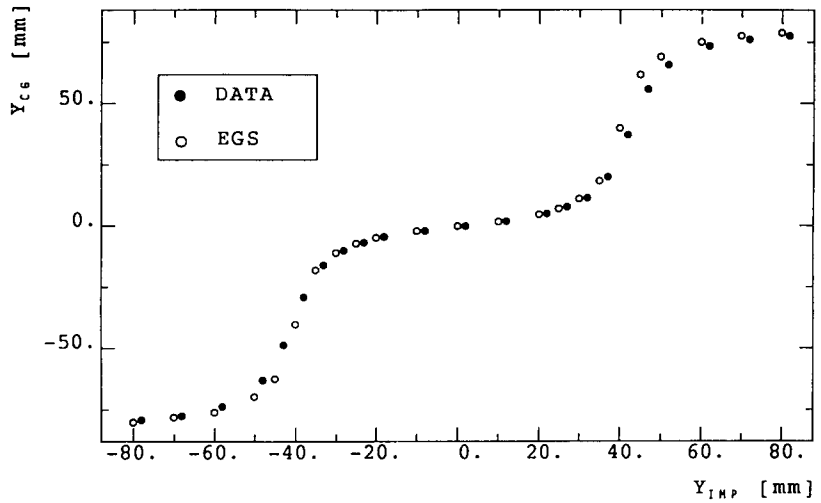

Fig. 18. Reconstructed centre of gravity as a function of the impact point for 3 GeV data (black circles) and the EGS prediction (open circles).

$(1.4 \pm 0.1)\%$ has been substracted from the high energy data. A fit to the combined data results in

$$\frac{\sigma_E}{E}[\%] = \sqrt{(1.0 \pm 0.06)^2 + \frac{(1.6 \pm 0.08)^2}{E[\mathrm{GeV}]}} \,. \qquad (6)$$

The energy dependent term of the resolution function is mainly determined by the low energy data, whereas the constant term, giving an approximate description of the leakage fluctuations, is fixed by the data taken at high electron energies.

3.5. Spatial resolution

To determine the spatial resolution of the calorimeter, a vertical scan along the y-axis (see fig. 3) has been performed with an electron beam. The pulse heights of three counters are plotted in fig. 16 as a function of the impact point. Due to lateral leakage, the shower signal is shared by neighbouring counters. The minima observed in fig. 16 appear at the position of the planes separating different scintillating glass modules. Summing up the signal detected in all counters of the matrix

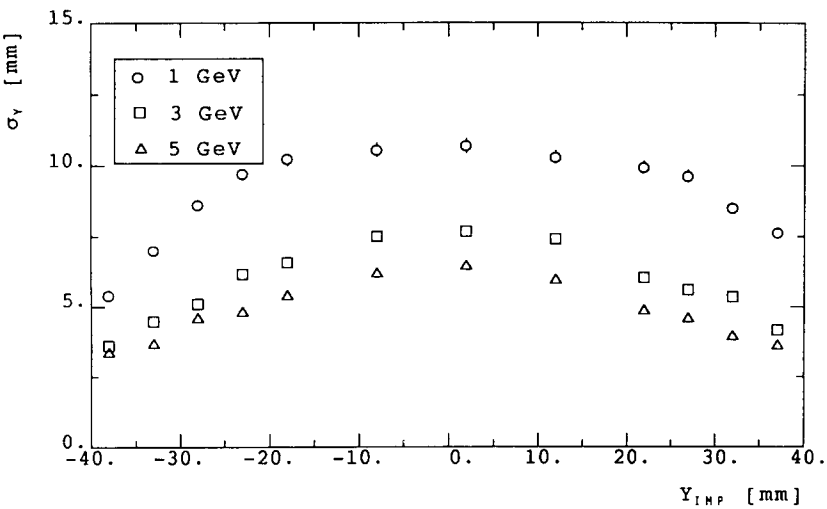

Fig. 19. Measured spatial resolution as a function of the impact point for three different energies.

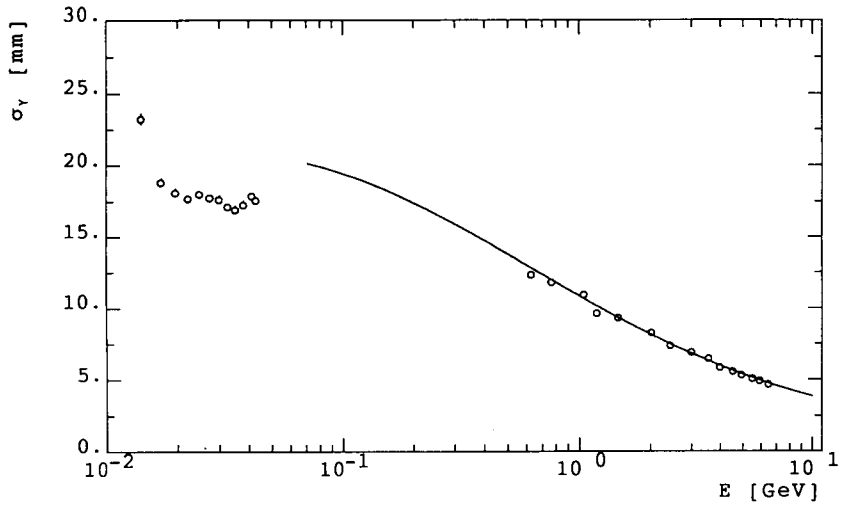

Fig. 20. Measured spatial resolution as a function of the energy. The curve shows parametrization (8) described in the text.

a homogeneous overall response is observed. The leakage of the shower into modules neighbouring the counter hit by the electron can be exploited to determine the impact point of the photon with a higher precision than expected from the lateral dimensions of the modules. In fig. 17 we hace plotted the centre of gravity

$$y_{\mathrm{COG}} = \frac{\sum \mathrm{PH}_i y_i}{\sum \mathrm{PH}_i}, \tag{7}$$

with

PH_i = recorded pulse height in counter i,

y_i = central coordinate in horizontal (vertical) direction of counter i,

as a function of the impact point y_{imp} for three different energies ($E = 1$, 3, 5 GeV). The curves fall on top of each other. In fig. 18 we have compared the data recorded at $E = 1$ GeV with the distribution expected from a shower Monte Carlo calculation, which coincides within the error limits with the data. One can use the correlation observed in fig. 17 to invert the problem and derive on an event basis the impact point y_{imp} from the measured value of y_{COG}, once one has found a parametrization of the observed correlation. The spatial resolution of the matrix achieved is given in fig. 19 for three energies as a function of the impact point in the central module. Note that the electrons in the experiment impinge orthogonal to the transverse plane of the module. The experimental results agree with the expectation derived from a Monte Carlo simulation. From this study and from a comparison with shower counter modules of different size [2] we conclude that the spatial resolution depends on impact point, counter size and energy of the incoming particle. Its energy dependence is shown in detail in fig. 20. Note that at high energies the spatial resolution follows an $1/\sqrt{E}$ dependence due to the statistical fluctuations of the leakage. At small energies the achieved resolution is better than the resolution of 8 cm/$\sqrt{12}$ expected from the fact that it is possible to identify the module which was hit by the incident particle. The function

$$\sigma_y[\mathrm{cm}] = \frac{a}{\sqrt{bE + 1}}, \tag{8}$$

with

$a = (8 \pm 0.3)$ cm/$\sqrt{12}$,

$b = (3.3 \pm 0.3)$ GeV^{-1},

is a reasonable parametrization of the observed resolution at high energies.

3.6. Long term stability

The deterioration of the scintillating glass by radiation is a potential danger and might inhibit its use in a storage ring experiment. Therefore the radiation damage was studied by iradiating $3 \times 3 \times 3$ cm^3 glass blocks with the Dortmund betatron [19]. The radiation damage was recorded by measuring the light output produced by cosmic rays in the glass block, the efficiency of the photomultipliers was monitored with a LED. Three different measurements were performed depositing an integrated dosis of 2150, 4300 and 6440 Gy respectively. No change of the light output within the reproducibility of the measurement ($\pm 3\%$) was observed. The expected integral dosis in a storage ring experiment is much lower than the values given above, hence no deterioration of the scintillating glass should arise from this potential source of danger during the course of an experiment.

4. Summary

In summary, we have tested the new scintillating glass HED-1 in the energy region 14.7 MeV $< E <$ 6000

Table 3
Energy and spatial resolution achieved for different types of homogeneous shower counters

	HED-1	SCG1-C	SF5	SF6	CsI(Tl)
σ_E/E [%]	$\sqrt{1.6^2/E+1.0^2}$	$2.4/\sqrt{E}$ [9]	$4.2/\sqrt{E}$ [11,20]	$3.6/\sqrt{E}$ [21]	$\sqrt{(1.3/\sqrt{E}+0.7E^{0.3})^2+(0.3/E)^2}$ [3]
E [GeV]	$0.015 < E < 6$	$0.02 < E < 0.12$	$0.02 < E < 100$	$0.3 < E < 90$	$0.04 < E < 5$
σ_E/E [%]		$1.46/E+1.63$ [13]			$2.8/\sqrt{E}$ [4]
E [GeV]		$1 < E < 25$			$0.2 < E < 1.5$
σ_y [cm]	$2.3/\sqrt{3.3E+1}$				$1.4/\sqrt{5E+1}$ [3]
E [GeV]	$1 < E < 6$				$0.3 < E < 5$

MeV. As far as linearity, energy and spatial resolution are concerned, this glass has properties of an almost ideal calorimeter. The observed behaviour of the electromagnetic calorimeter agrees with the expectation based on the simulation of the shower development (EGS), the light collection and the photoelectron statistics, the latter being of special importance at the lowest energies. Compared to other homogeneous shower detectors as BGO, CsI(Tl), BaF_2 and NaI(Tl) this glass has the disadvantage of larger radiation length (factor 2 to 3) and less light output (factor 50 to 500). However, this can be compensated by replacing the photodiodes used for the readout by a photomultiplier, which results in a comparable energy resolution (table 3) even at low energies at a much lower price (factor 10 to 20). Scintillating glass (HED-1) is superior due to its perfect homogeneity which can be of high importance, as demonstrated by the fact that for BGO at 40 MeV resolutions between 1.7% and 8% have been reported [5], the latter is comparable to the results of the present investigations. An additional advantage is the high radiation resistance of the glass and its short decay constant (factor 3 to 10). The last fact is of special advantage for multibunch machines as foreseen in B-factories.

Acknowledgements

It is a pleasure to thank Dr. U. Matthiesen for his assistance with the data acquisition. This work has been supported by the Bundesministerium für Forschung und Technologie, FRG, under contract number 054DO051p.

References

[1] CLEO II Updated Proposal, CLNS-85/634.
[2] J. Spengler, Proc. Int. Symp. on Production and Decay of Heavy Hadrons, Heidelberg (1986) p. 448.
[3] E. Blucher et al., Nucl. Instr. and Meth. A249 (1986) 201.
[4] T. Adachi et al., Nucl. Instr. and Meth. A254 (1987) 270.
[5] E. Lorenz, Proc. 3rd Int. Conf. on Instrumentation for Colliding Beam Physics, Novosibirsk (1984).
[6] Schott GmbH, Mainz, FRG.
[7] Ohara Optical Glass Inc., Watching, NJ 07060, USA.
[8] Y. Yoshimura et al., Nucl. Instr. and Meth. 137 (1976) 57.
[9] M. Kobayashi et al., Nucl. Instr. and Meth. 184 (1981) 399.
[10] M. Kobayashi et al., Nucl. Instr. and Meth. 196 (1982) 239.
[11] M. Chiba et al., Nucl. Instr. and Meth. A234 (1985) 267.
[12] B. Cox et al., Nucl. Instr. and Meth. 219 (1984) 487.
[13] D.E. Wagoner et al., Nucl. Instr. and Meth. A238 (1985) 315.
[14] U. Amaldi, Phys. Scripta 23 (1981) 409.
[15] G. Schweda, Diplomarbeit, Universität Dortmund (1987).
[16] U. Buchner, Diplomarbeit, Universität Dortmund (1988).
[17] LeCroy 2282A and 2249W.
[18] W.R. Nelson et al., The EGS4 Code System, SLAC-265 (1985).
[19] M. Kaiser, Diplomarbeit, Universität Dortmund (1986).
[20] S. Bartalucci et al., Nucl. Instr. and Meth. 178 (1980) 401.
[21] S. Orito et al., Nucl. Instr. and Meth. 215 (1983) 93.